Cubane core / 1D polynuclear copper(II) complexes: Structure, protein / DNA binding and magnetic properties

Aparup Paul,[a] C. M. Nagaraja,[b] Albert Figuerola [c,d] Subal Chandra Manna[a]

[a]*Department of Chemistry and Chemical Technology, Vidyasagar University, Midnapore 721102, West Bengal, India, E-mail: scmanna@mail.vidyasagar.ac.in, Fax: (91) (03222) 275329.*

[b]*Department of Chemistry, Indian Institute of Technology, Ropar, Punjab 140001, India.*

[c]*Institut de Nanociència i Nanotecnologia (IN2UB), Universitat de Barcelona, Martí i Franquès 1-11, 08028 Barcelona, Spain.*

[d]*Departament de Química Inorgànica i Orgànica, Secció de Química Inorgànica, Universitat de Barcelona, Martí i Franquès 1-11, 08028 Barcelona, Spain.* [e]~~*Departament de Química Inorgànica i Orgànica (Secció de Química Inorgànica) and Institut de Nanociència i Nanotecnologia (IN2UB), Universitat de Barcelona, Martí i Franquès 1-11, 08028 Barcelona, Spain.*~~

Formatat: Tipus de lletra: Cursiva, No Superíndex/ Subíndex

Formatat: Tipus de lletra: Cursiva, No Superíndex/ Subíndex

Formatat: Tipus de lletra: Cursiva, No Superíndex/ Subíndex

Formatat: Tipus de lletra: Cursiva, No Superíndex/ Subíndex

Formatat: Tipus de lletra: Cursiva, No Superíndex/ Subíndex

Formatat: Tipus de lletra: No Superíndex/ Subíndex

Abstract

Two novel tetranuclear copper(II) complexes namely $[Cu_4(L^1)_4]\cdot(H_2O)$ (**1**), $[Cu_4(L^2)_2(HL^2)_2(H_2O)_2]\cdot(Sq)\cdot 3(H_2O)$ (**2**) and one 1D polymeric copper(II) complex $\{[Cu_2(L^2)_2(tp)]\cdot(H_2O)\}_n$ (**3**) have been synthesized from two potentially Schiff base ligands H_2L^1 and H_2L^2 (H_2L^1= [(E)-2-((1-hydroxybutan-2-ylimino)methyl)phenol], H_2L^2 =[(E)-2-((1-hydroxybutan-2-ylimino)methyl)-6-methoxyphenol], Sq = Squarate ions and tp = terephthalate ions). The structural determination reveals that complex **1** crystallizes in the triclinic system with space group *P-1*, whereas both the complexes **2** and **3** crystallize~~s~~ in the monoclinic system with space group *P21/n* and *Pn*-, respectively. Both **1** and **2** present~~s~~ a cubane-like core structure (Cu_4O_4) with ~~two~~ different ~~types~~ [4+2] geometry~~,~~: **1** possesses four short and two long Cu···Cu distances as a result of the particular relative arrangement of the axial axes and equatorial planes of the Cu(II) ions, leading to a [4+2] geometric type of close cubane. ~~but~~ On the contrary,

Comentat [AFS1]: What do you mean by potentially???

complex **2** belongs to a specific type of [4+2] cubane compound where one of the two long Cu···Cu distances is formed by a Cu(II)-Cu(II) pair not connected through a bridging ligand, and leading to a [4+2] double-open cubane structure. On the other hand, complex **3** consists of one dimensional polymeric chains formed by the linkage of the asymmetric dinuclear unit through terephthalate ions. The copper(II) ions in **3** are in distorted octahedral geometries, and weak C-H…π interactions lead to formation of a 3D supramolecular architecture. At room temperature all the complexes exhibits fluorescence with a quantum yield (Φ_s) of 0.39 (for **1**), 0.51(for **2**) and 0.37 (for **3**). Variable temperature magnetic susceptibility calculations in the range 2 - 300 K indicate an overall weak antiferromagnetic exchange coupling in all complexes. The PHI program was used to study their magnetic behavior. In agreement with their [4+2] cubane structure, a Hamiltonian of the type $H = -J_1 (S_1S_2 + S_1S_4 + S_2S_3 + S_3S_4) - J_2 (S_1S_3 + S_2S_4)$ and $H = -J_1 (S_1S_3 + S_2S_4) - J_2 (S_1S_2 + S_3S_4) - J_3S_1S_4$ were used for studying **1** and **2** respectively and a good agreement between the experimental and simulated results were found by using parameters $g = 2.14$, $J_1 = -20.2$ cm^{-1} and $J_2 = -1.7$ cm^{-1} (for **1**) and $g_1 = 2.14$, $g_2 = 2.12$, $J_1 = -54.8$ cm^{-1}, $J_2 = -15.9$ cm^{-1} and $J_3 = 0$ cm^{-1} (for **2**). The analysis of the magnetic data of **3** can be carried out by using a simple dinuclear model with anisotropic Hamiltonian of the type: $H = -J (S_1S_2)$, where J describes the magnetic exchange operating between the two Cu(II) ions in the asymmetric dinuclear unit and a good agreement with the experimental curve was found with the parameters: $g = 2.08$ and $J = -0.5$ cm^{-1}. The interactions of complexes with bovine serum albumins (BSA), human serum albumin (HSA) and calf thymus DNA (CT-DNA) were studied using electronic absorption and fluorescence spectroscopic techniques. The results show that the interaction of complexes with BSA / HSA occurs mainly with ground state association process, and interacted with CT-DNA through intercalation.

Introduction

High nuclearity copper(II) complexes have attracted much attention because of their interesting architectures and potential applications in different fields such as molecular magnetism,[1] bioinorganic chemistry,[2] coordination polymers[3] and catalysis.[4]Among them, tetranuclear cubane-type copper(II) complexes (Cu_4O_4) draw special attention due to their magnetic properties,[5] along with as a model system for metallo-enzymes.[6] Two classification of Cu_4O_4 core have been suggested on the basis of their structural features. The first one was proposed by Mergehem and Haase,[7] they classified cubane cores into two types (I and II), depending on the length of the Cu-O bonds within the cubane core. Cubane complexes having four long Cu-O distances between two dinuclear subunits are classified as type-I, whereas cubane complexes having long Cu-O distances within each dinuclear subunit are classified as type-II. The second one is based on the Cu…Cu distances within the cubane core, proposed by Ruiz et al.[8] According to them cubanes have been classified into three categories: (i) [2+4] with two short and four long Cu…Cu distances, (ii) [4+2] four short and two long Cu…Cu distances and (iii) [6+0] contains six similar Cu…Cu distances. The structure and geometry of polynuclear copper(II) complexes are very important, as the magnetic behavior~~s~~ of ~~the~~ copper complexes ~~are~~ is closely related with their structure, with slight changes in structure ~~causes~~ causing significant ~~change~~ modifications ~~in~~ of their magnetic ~~behavior~~properties.

Polynuclear copper complexes are also found in biological systems in the form of oxidase enzymes.[9] Being a bio-essential metal ion, copper is involved in many biological processes and plays a significant role in the regular function of cells.[10] Well-defined redox active copper(II) complexes might be efficient antioxidants, antimicrobials, antiparasitics and antitumor agents.[11] Lots of mixed ligand copper(II) compounds have been found to be excellent anticancer agents as they induce apoptosis due to their effective DNA binding / cleaving ability.[12] To understand the potential of copper compounds as drugs, studies on the binding of complexes to plasma proteins is a crucial step, because therapeutic efficiency, drug delivery

and drug absorption ~~are~~ closely depend~~s~~ on the nature and magnitude of these binding.[13] For that reason, understanding and characterizing the interactions of complexes with serum albumins (SAs) are important to serve as a drug. Like magnetic behaviors, the performance of copper complexes as mettalo-drugs, depends on their ligand framework, oxidation state of copper ions, coordination geometry of the copper complexes and their possible interaction with biomolecules.[14] The organic ligands introduced into the complex could control metal uptake, function and excretion in biological systems that may limit the side effects and provide better activities in drug resistance cells.[15] Schiff base ligands, are known to be an important class of compounds with various pharmacological activities including anticancer, antibacterial and antiviral activity.[16] Schiff base copper complexes may promote the production of reactive oxygen species (ROS), which in turn subsequently induces DNA damage and mitochondria dysfunctions and finally stimulates apoptosis.[17] On the other hand introduction of co-ligands may affect the planarity and hydrophobicity as well as the coordination geometry of the copper complexes and in due course enhance the DNA binding affinity of copper complexes.[15, 18]

Taking into consideration the significance of copper-Schiff base compounds in molecular magnetism and in medicinal chemistry, our recent studies have been focused on the interaction of Schiff base-copper complexes with bio-molecules (DNA / SAs) as well as their magneto-structural relationship.

So as a part of our continuing work on the synthesis, characterization and application of copper complexes with Schiff base, herein we report the synthesis and characterization of three new Schiff base copper(II) polynuclear complexes (two cubanes with a Cu_4O_4 core belonging 4+2 class and one 1D polymeric copper complex), namely $[Cu_4(L^1)_4]\cdot(H_2O)$ (**1**), $[Cu_4(L^2)_2(HL^2)_2(H_2O)_2]\cdot(Sq)\cdot 3(H_2O)$ (**2**) and $\{[Cu_2(L^2)_2(tp)]\cdot(H_2O)\}_n$ (**3**) [H_2L^1 = [(E)-2-((1-hydroxybutan-2-ylimino)methyl)phenol], H_2L^2 = [(E)-2-((1-hydroxybutan-2-ylimino)methyl)-6-methoxyphenol], Sq = Squarate ions and tp = terephthalate ions]. Although both the Schiff

base ligands ~~has~~ were previously ~~been~~ utilized in the synthesis of some mononuclear, binuclear, and polynuclear structures[19] with 3d transition metals, ~~but~~ a Cambridge Database (CCDC) search reveals that so far few cubane-like clusters were reported using these Schiff base ligands, and they mainly focused on magneto-structural relationship but interactions with biomolecules are quite rare. So in order to enrich the family of Schiff base - copper(II) polynuclear complexes we ~~were~~ studied the variable temperature magnetic measurements of these complexes as well as the interactions with CT-DNA and Serum albumins (BSA / HSA) using electronic absorption and emission spectral techniques.

Experimental

Materials and measurements

High purity 2-Amino-1-butanol, ethidium bromide (EB), human serum albumin (HSA), bovine serum albumin (BSA) and calf thymus DNA (CT-DNA) were obtained from Aldrich Chemical Co. Inc. All other chemicals used were analytical grade. Solvents used for spectroscopic studies were purifies and dried by standard procedures before use.[20] Elemental analyses (carbon, hydrogen and nitrogen) were performed using a Perkin-Elmer 240C elemental analyzer. IR spectra were recorded as KBr pellets on a Bruker Vector 22FT IR spectrophotometer operating from 400 to 4000 cm^{-1}. Electronic absorption spectra were obtained with Shimadzu UV-1601 UV-vis spectrophotometer at room temperature. Quartz cuvettes with a 1 cm path length and a 3 cm^3 volume were used for all measurements. Emission spectra were recorded on a Hitachi F-7000 spectrofluorimeter. Room temperature (300 K) spectra were obtained using a quartz cell of 1 cm path length. The slit width was 2.5 nm for both excitation and emission. The fluorescence quantum yield was determined using phenol as a reference and methanol medium for both complexes and reference. Emission spectra were recorded by exciting the complex and the reference phenol at the same wavelength, maintaining nearly equal absorbance (~ 0.1).

The area of the emission spectrum was integrated using the software available in the instrument and the quantum yield calculated[21] according to the following equation:

$$\Phi_s = \Phi_r \frac{A_s}{A_r} \frac{I_r}{I_s} \frac{\eta_s^2}{\eta_r^2}$$

Where Φ_s and Φ_r are the fluorescence quantum yield of the sample and reference, respectively. A_s and A_r are the respective optical densities at the wavelength of excitation, I_s and I_r correspond to the areas under the fluorescence curve; and η_s and η_r are the refractive index values for the sample and reference, respectively. The fluorescence enhancement efficiency (%) was calculated by using equation $[(F - F_o)/F_o] \cdot 100$ and the corresponding quenching efficiency (%) by $[(F_o - F)/F_o] \cdot 100$, where F_0 and F are the maximum fluorescence intensity of the complex before exposure and in presence of the analyte, respectively. Temperature-dependent molar susceptibility measurements of polycrystalline samples were carried out at the Servei de Magnetoquímica of the Centres Científics i Tecnològics at the Universitat de Barcelona in a Quantum Design SQUID MPMSXL susceptometer with an applied field of 3000 and 198 G in the temperature ranges 2 - 300 and 2 - 30 K, respectively.

Synthesis of the ligands

The ligands [(E)-2-((1-hydroxybutan-2-ylimino)methyl)phenol] (H_2L^1) and [(E)-2-((1-hydroxybutan-2-ylimino)methyl)-6-methoxyphenol] (H_2L^2) were prepared by the same general procedure.

H_2L^1. A methanolic solution of 1:1 mixture of 2-aminobutanol and 2-hydroxy benzaldehyde was refluxed for 3 h. The resulting yellow color solution was cooled to room temperature and solid yellow compound was obtained after evaporation of solvent. Re-crystallization of compound using methanol as solvent resulted yellow crystalline compound. Crystalline solid was collected by filtration and dried in air to afford H_2L^1. Yield: 0.164 g (85%). *Anal*. Calc. for

$C_{11}H_{15}NO_2$ (193.24): C, 68.36; H, 7.82; N, 7.24 %. Found: C, 68.34; H, 7.79; N, 7.26 %. ^{1}H NMR (400 MHz, $CDCl_3$, δ ppm): 0.709 - 0.886 (3H, m), 1.474 - 1.655 (2H, m), 2.576 (1H, s), 3.466 - 3.690 (1H, m; 2H, m), 4.957 (1H, s), 6.823 - 6.921 (1H, d; 2H, m), 7.226 - 7.298 (1H, d; 2H, m), 8.306 (1H, s). ^{13}C NMR ($CDCl_3$, 400 MHz, δ ppm): 165.41 (Ar-C-OH), 161.71 (-CH=N-), 132.45 - 113.71 (Ar-C), 73.03 (-CH_2-OH), 66.23 (=N-CH-), 25.05 (-CH_2-), 10.51 (-CH_3).

H_2L^2. Yellow color ligand was synthesized adopting the same procedure as for H_2L^1, using 2-hydroxy-3-methoxy benzaldehyde instead of using 2-hydroxy benzaldehyde. Yield: 0.187 g (84%). *Anal*. Calc. for $C_{12}H_{17}NO_3$ (223.26): C, 64.49; H, 7.61; N, 6.27 %. Found: C, 64.48; H, 7.63; N, 6.28 %. ^{1}H NMR (400 MHz, $CDCl_3$, δ ppm): 0.900 (3H, m), 1.515 - 1.667 (2H, m), 2.353 (1H, s), 3.169 - 3.208 (1H, m), 3.607 - 3.895 (2H, d; 3H, s), 4.867 (1H, s), 6.689 - 6.941 (1H, d; 2H, m; 1H, d), 8.279 (1H, s). ^{13}C NMR ($CDCl_3$, 400 MHz, δ ppm): 148.70 (Ar-C-OH), 165.46 (-CH=N-), 124.53 - 113.96 (Ar-C), 72.12 (-CH_2-OH), 65.61 (=N-CH-), 56.27 (-O-CH_3), 24.97 (-CH_2-), 10.39 (-CH_3).

Scheme1. Structures of H_2L^1 and H_2L^2 with their coordination modes in **1-3**

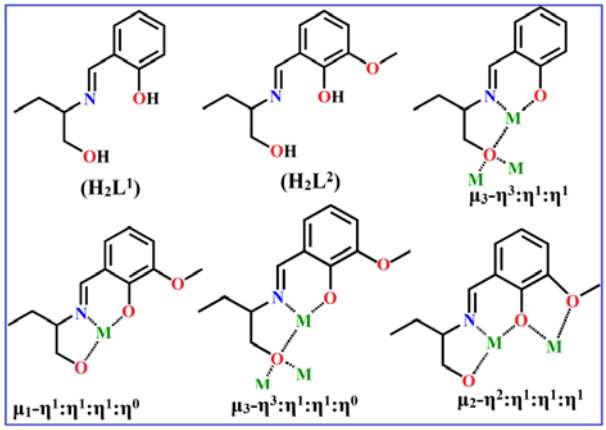

Synthesis of complexes

Caution! Perchlorate salts of metal with organic ligands are potentially explosive. Only a small amount of material should be prepared, and it should be handled with care.

The complexes have been synthesized by adopting the procedures schematically given in Scheme 2.

Scheme 2 Synthesis of **1**, **2** and **3**

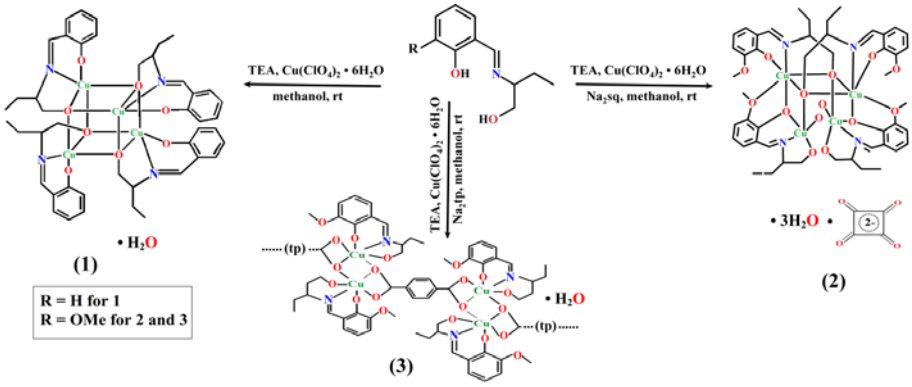

$[Cu_4(L^1)_4].(H_2O)$ (1). A methanolic solution (5 mL) of triethylamine (1 mmol, 0.101 g) was added drop wise to a methanolic solution (10 mL) of H_2L^1 (1 mmol, 0.193 g) in stirring condition for 5 min. To this resulting mixture, drop wise addition of methanolic solution (10 mL) of copper perchlorate hexahydrate (1 mmol; 0.370 g) yielding a deep green solution. The whole reaction mixture was stirred for 2 hours and filtered. The filtrate was kept in open atmosphere for slow evaporation and green single crystals suitable for X-ray diffraction quality were obtained after a few days. Yield: 78 %. *Anal.* Calc. for $C_{45}H_{54}Cu_4N_4O_9$ (1049.08): C, 51.51; H, 5.18; N, 5.34 %. Found: C, 51.13; H, 5.13; N, 5.42 (%). IR (cm^{-1}): 3430 (vs), 2981 (vw), 1641 (vs), 1553 (vs), 1467 (s), 1414 (vs), 1373 (w), 1300 (s), 1195 (vw), 1151 (vw), 1113 (vw), 1078 (s), 1014 (vw), 881(vw), 817 (vw), 763 (vw), 636 (vw).

$[Cu_4(L^2)_2(HL^2)_2(H_2O)_2]\cdot(Sq)\cdot 3(H_2O)$ (**2**) and $\{[Cu_2(L^2)_2(tp)]\cdot(H_2O)\}_n$ (**3**).

A methanolic solution (5 mL) of triethylamine (1 mmol, 0.101 g) was added drop wise to a methanolic solution (10 mL) of H_2L^2 (1 mmol, 0.223 g) in stirring condition for 5 min. To this resulting mixture, drop wise addition of methanolic solution (10 mL) of copper perchlorate hexahydrate (1 mmol; 0.370 g) yielding a deep green solution. To the resulting green solution an aqueous solution of sodium squarate for **2** (1 mmol, 0.158 g) and sodium terephthalate for **3** (1 mmol, 0.210 g) were added after 2 hours and stirred additional 1 hour and filtered. For **2**: Yield: 81%. *Anal.* Calc. for $C_{52}H_{57}Cu_4N_4O_{21}$ (1328.17): C, 47.02; H, 4.32; N, 4.21 %. Found: C, 46.77; H, 4.37; N, 4.11 (%). IR (cm^{-1}): 3435 (vs), 2981 (vw), 1642 (vs), 1553 (vs), 1466 (s), 1413 (vs), 1373 (s), 1299 (s), 1246 (vw), 1216 (vw) 1078 (s), 1053 (vw), 974(w), 881 (vw), 741 (vw), 640 (vw).

For **3**: Yield: 77 %. *Anal.* Calc. for $C_{32}H_{34}Cu_2N_2O_{11}$ (749.69): C, 51.26; H, 4.57; N, 3.73 %. Found: C, 51.03; H, 4.54; N, 3.75 (%). IR (cm^{-1}): 3429 (vs), 2983 (w) 1644 (vs), 1552 (vs), 1467 (s), 1414 (vs), 1373 (s), 1299 (s), 1245 (w), 1218 (vw), 1079 (s), 975 (w), 882(vw), 781 (vw), 635 (vw).

Crystallographic data collection and refinement

X-ray single crystal structural data of compounds **1**-**3** were collected on a Bruker D8 Venture PHOTON 100 CMOS diffractometer equipped with a INCOATEC micro-focus source and graphite monochromated MoKα radiation (λ = 0.71073 Å) operating at 50 kV and 30 mA. The program SAINT[22] was used for integration of diffraction profiles and absorption correction was made with SADABS[23] program. All the structures were solved by SIR 92[24] and refined by full matrix least-square method using SHELXL-2013[25] and WinGX system (ver 2013.3).[26] All the non hydrogen atoms were located from the difference Fourier map and refined anisotropically. All the hydrogen atoms were fixed by HFIX and placed in ideal positions and included in the refinement process using riding model with isotropic thermal parameters. Packing diagrams were done with graphical program Diamond.[27] All the crystallographic and

structure refinement data of compounds **1-3** are summarized in Table 1. Selected bond lengths and angles are given in Tables 2, 1S-3S.

Protein binding studies

Stock solutions of human serum albumin (HSA) and bovine serum albumin (BSA) were prepared in HEPES buffer (pH 7.2) solution. Aqueous solutions of **1-3** were prepared by dissolving the compounds in water: HEPES buffer (1:99). The absorption titration experiments were carried out by keeping the concentration of SAs constant (4.75×10^{-5} M for BSA and 3.33×10^{-5} M for HSA), while varying the concentrations of Cu(II) complexes (0 to 11.2 µM). The interactions of compounds with serum albumins were studied by recording the tryptophan fluorescence of BSA / HSA. To the solutions of serum albumin, Cu(II) complexes were added at room temperature, and the quenching of emission intensities at 340 nm (λ_{ex}, 280 nm) for BSA and 330 (λ_{ex}, 280 nm) for HSA were recorded after gradual addition of (20 µL, 0.3475 mmol) aqueous solution of complexes. The Stern-Volmer constant (K_{sv}) and quenching rate constant (k_q) were calculated using the equations $F_0/F = 1 + K_{sv}[complex]$ and $K_{sv} = k_q\tau_0$, where F_0 and F are the fluorescence intensities in the absence and in the presence of the complex, and τ_0 is the lifetime of serum albumin (~ 5×10^{-9} s).[28] The binding constant (K_{bin}) and the number of binding sites (n) are calculated using the following Scatchard equation.[29]

$$\log[(F_o–F)/F] = \log K_{bin} + n \log[complex]$$

DNA binding studies

Electronic absorption spectral study

The binding of complexes **1-3** with CT-DNA was studied by electronic absorbance spectroscopy to investigate the possible DNA-binding modes and to calculate the intrinsic binding constant (K_{ib}) for the interaction of the compounds with CT-DNA. In electronic absorption spectral titration the UV spectra of each complex (5 µM) were recorded with gradual

addition of 20 µL, 0.3059 mmol CT-DNA solution. Intrinsic binding constant (K_{ib}) of the complex with CT-DNA was determined using the equation[30]

$$\frac{[DNA]}{(\varepsilon_a - \varepsilon_f)} = \frac{[DNA]}{(\varepsilon_b - \varepsilon_f)} + \frac{1}{K_{ib}(\varepsilon_b - \varepsilon_f)}$$

Where [DNA] is the concentration of CT-DNA, ε_a is the extinction co-efficient value of the complex at a given CT-DNA concentration, ε_f and ε_b are the extinction co-efficient of the complex only and when fully bound to CT-DNA, respectively. The plot of [DNA]/($\varepsilon_a - \varepsilon_f$) vs [DNA] gives a straight line with $\frac{1}{(\varepsilon_b - \varepsilon_f)}$ and $\frac{1}{K_{ib}(\varepsilon_b - \varepsilon_f)}$ as slope and intercept, respectively. From the ratio of the slope to the intercept the value of K_{ib} was calculated.

Competitive binding fluorescence measurement

The competitive binding nature of ethidium bromide (EB = 3, 8-diamino-5-ethyl-6-phenyl phenanthridinium bromide) and copper(II) compounds, with CT-DNA were studied adopting fluorometric method on gradual addition of copper(II) complexes (20µL, 0.3475 mmol) to aqueous solution (5 µM) of EB bound CT-DNA in HEPES buffer (pH 7.2) at room temperature. In presence of CT-DNA, EB exhibits fluorescence (λ_{em} = 602 nm, λ_{ex} = 500 nm) enhancement due to its intercalative binding to DNA. Competitive binding of copper(II) compounds with CT-DNA results fluorescence quenching due to displacement of EB from CT-DNA. The Stern-Volmer constant (K_{sv}) was calculated using Stern-Volmer equation[21] $F_0/F = 1 + K_{sv}[complex]$, where F_0 and F are the emission intensities in absence and in presence of copper(II) compounds, K_{sv} is the Stern-Volmer constant, and [complex] is the concentration of copper (II) complexes.

Results and discussion

Crystal structure description

$[Cu_4(L^1)_4] \cdot H_2O$ (1)

The molecular structure of **1** is shown in Fig. 1. Details crystal structure refinement, selected bond lengths and angles as well as inter-metallic distances are listed in Tables 1-2, 1S-2S. Complex **1** crystallizes with triclinic crystal system and *P-1* space group and consists of tetrameric $[Cu_4(L^1)_4]$ moiety with one lattice water molecule. The tridentate Schiff base ligand (H_2L^1) which can adopt both chelating and bridging modes (Scheme 1) undergoes double deprotonation upon addition of triethyl amine (TEA) and the dianionic form of ligand coordinates to the copper(II) centers through the deprotonated alkoxo oxygen, phenolic oxygen and imine nitrogen atoms via μ_3-η^3:η^1:η^1 coordination mode. The neutral tetranuclear complex **1** formed by the self-assembly process of four $[CuL^1]$ units (Fig. 1). The cubane structure is characterized by a Cu_4O_4 core where the anionic alkoxo-oxygen atoms connecting three neighboring Cu(II) ions via μ_3-O bridges (Fig. 2). The vertices of the cube are occupied by four Cu(II) and four μ_3-bridging alkoxide oxygen atoms in alternating fashion. All Cu(II) centers have five coordination number with NO_4 donor set from the Schiff base ligands. For a penta coordinated metal center, the distortion of the coordination environment from trigonal bipyramidal to square pyramidal can be evaluated by the Addison distortion index (τ), defined as the $\tau = [(\beta-\gamma)/60]$, where β and γ are the two largest coordination angles around the metal[31] (τ is zero for the perfect square pyramid while it becomes unity for an ideal trigonal bipyramidal geometry). The coordination geometry around each Cu(II) center is distorted square pyramidal as reflected from the respective τ values (τ = 0.207 for Cu1, τ = 0.208 for Cu2, τ = 0.220 for Cu3 and τ = 0.132 for Cu4). The basal plane of the square pyramid is formed by the phenolate oxygen atom, the imine nitrogen atom and two μ_3-alkoxide oxygen atoms, while the apical position occupied by another μ_3-alkoxide oxygen atom. Cu1, Cu2, Cu3 and Cu4 are deviated from the corresponding mean planes by 0.1046, 0.0987, -0.0818 and -0.0711Å respectively, towards the apical ligand atom. The Cu-O and Cu-N bond lengths in the equatorial plane vary from 1.882(4) to 1.973(3) Å and from 1.933(4) to 1.947(4) Å, respectively (Table 2). The apical

oxygen atoms show longer Cu-O bond lengths ranges between 2.504(3) to 2.607(3) Å due to the pseudo Jahn-Teller distortion of the d^9 copper center. The Schiff base ligand $[(L^1)^{2-}]$ act as a tridentate ligand for one copper(II) ion leading to five and six-membered chelate rings with average bite angles of 83.85 and 94.03° respectively. The bridging bond angles of Cu-O-Cu are between 87.79(12) - 113.22(13)° (Table 2S). From the Cu-O body diagonal distances and Cu-Cu distances it is evident that the cubane is distorted not regular. Based on Cu...Cu distance, Cu_4O_4 core have been classified as (i) (2+4), where Cu...Cu distances are two short and four long; (ii) (4+2) where Cu...Cu distances are two long and four short; and (iii) (6+0), all Cu...Cu distances are identical.[8] In the core structure of complex **1** four Cu...Cu distances are short and two are long (Table 1S) and hence core Cu_4O_4 of **1** can be classified as (4+2) system.

$[Cu_4(L^2)_2(HL)_2(H_2O)_2]\cdot(Sq)\cdot 3(H_2O)$ (2)

The crystal structure of **2** is shown in Fig. 3. The compound crystallizes with monoclinic crystal system and P21/n space group with four molecules in the unit cell. Selected bond lengths and angles as well as inter-atomic distances are summarized in Tables 2,1S - 2S. The core symmetry of complex **2** possesses double-open cubane structure (Fig. 1S). The cationic complex contain four copper(II) centers, two dideprotonated ligands $[(L^2)^{2-}]$ in which both the phenol and alcohol moieties are deprotonated, two monodeprotonated ligands $[(HL^2)^-]$ in which only the phenoxido moiety is deprotonated and two coordinated water molecules. The charge of the cationic complex neutralize by a squarate lattice. Beside one squarate lattice, three lattice water molecules also present. Each mono deprotonated ligand chelates two copper atoms *via* μ_2-η^2:η^1:η^1:η^1 - O, O, N, O coordination mode, while the double deprotonated ligands chelates Cu1 and Cu4 centers, and in addition connect the previous moieties with the μ_3-alkoxido group resulting μ_3-η^3:η^1:η^1:η^0 - O, N, O, O coordination mode, the methoxy oxygen O4 and O12 are remain uncoordinated. The pair of $(HL^2)^-$ and $(L^2)^{2-}$ are arranged in a head-tail fashion about the cubane-like core so that the complex presents a pseudo two-fold axis passing in between

Cu1 / Cu4 and Cu2 / Cu3. Fig. 1S shows a simplified representation of the coordination environment around the four copper centers. The metal ions Cu2 and Cu3 present a similar square pyramidal (τ = 0.101 for Cu2, τ = 0.099 for Cu3) geometry. The basal plane of the square pyramid formed by the imine nitrogen, the phenoxido and the alcoholic oxygen of one $(HL^2)^-$ and completed with the alkoxido oxygen (μ_3-bridging) from a $(L^2)^{2-}$. The coordinated water molecule occupied the apical position of the square pyramid.

The basal coordination bond distances for Cu2 and Cu3 (Table 2) are in between 1.935 - 1.982 Å. The bond lengths between oxygen atom of coordinated water and copper are somewhat more distant, being at 2.314 and 2.296 Å for Cu2 and Cu3 respectively (Table 2).

The bond angles between the successive coordinating equatorial atoms with Cu2 atom are 96.08°, 87.24°, 92.13° and 83.44° and the angles between the axial atom, Cu2 and equatorial atoms are 96.11°, 95.95°, 88.98° and 96.50° whereas in Cu3 the bond angles between the successive coordinating equatorial atoms with Cu3 are 95.82°, 87.42°, 92.39° and 83.48° and the angles between the axial atom, Cu3 and equatorial atoms are 93.84°, 98.54°, 90.34° and 93.16°.

The coordination environment of Cu1 and Cu4 are also similar, both the metal centre remains in distorted octahedral geometry. The basal plane of the octahedron formed by the imine nitrogen, the phenoxido and the alkoxido oxygen from one $(L^2)^{2-}$ ligand and μ_2-phenoxido oxygen of $(HL^2)^-$, the axial positions are the occupied by methoxy oxygen of same $(HL^2)^-$ and the alkoxido oxygen atom of another $(L^2)^{2-}$ ligand.

The equatorial bond distances fall in the range 1.902 - 2.010 Å, while the axial bond lengths vary from 2.382 to 2.510 Å due to the Jahn-Teller distortion. The Cu2-O8 (2.884 Å) and Cu3-O1 (2.984 Å) distances are rather long and responsible for the double open cubane core structure. The metal atoms are located at the vertices of a distorted tetrahedron with edge dimension varying from 3.184 to 3.765 Å. For the Cu1 and Cu4 the trans angles are lie between

71.79° to 113.58° and the cis angles ranges between 83.74° to 94.24°. Based on Cu...Cu distances (Table 1S) complex **2** also ~~is in~~belongs to the class of (4+2) ~~system~~ copper cubanes.

{[$Cu_2(L^2)_2(tp)$]· (H_2O)}$_n$ (3)

Complex **3** crystallizes in the monoclinic system with space group Pn. The asymmetric unit of complex **3** is shown in Fig. 2S. X-ray structural analysis of complex revealed that asymmetric unit contains two Cu(II) cations, two deprotonated Schiff base ligands [$(L^2)^{2-}$], one terephthalate (tp) ions and one lattice water molecule. It consists of one dimensional polymeric chains formed by the linkage of the asymmetric dinuclear unit shown in Fig. 4. Neighbouring dinuclear units are bridged by terephthalate ions. Both the copper atom (Cu1 and Cu2) presenting a distorted octahedral environment formed by a deprotonated tridentate (O, N, O) Schiff base ligand, and two oxygen atoms from one carboxylate group and another oxygen atom from other carboxylate group. The square plane of the octahedron is formed by the three donating atom of Schiff base (O1, O2, N1 for Cu1; O7, O8, N2 for Cu2) and one oxygen atom from carboxylate (O3 for Cu1; O6 for Cu2), whereas the apical positions are occupied by other two oxygen atoms of the carboxylate (O4, O6 for Cu1; O3, O5 for Cu2). The four basal donor atoms are almost coplanar with respect to their mean planes, with a maximum deviation of 0.2293Å for Cu1 and 0.1960 Å for Cu2. The deviation of Cu1 and Cu2 are -0.0163 and 0.0328Å from their respective mean planes toward the O4 and O3 respectively. The coordination environments of the two copper(II) ions are the slightly difference in value of bond lengths and angles due to the formation of 1D polymeric chain. The Cu-O bond lengths are varies from 1.905(3) Å to 2.687(3) Å, whereas Cu-N bond lengths are 1.925(3) Å and 1.922(4) Å. The distance between two copper atoms is 3.529 Å, indicating the absence of any bond between two copper centers. The largest bond angle in **3** is O(7)-Cu(2)-O(8) [171.57(13)°] whereas smallest bond angle is O(3)-Cu(1)-O(6) [76.51(11)°]. The Cu-O-Cu bridge angles are 97.78 Å and 102.42 Å. The packing diagram indicates that complex **3** exists as 1D polymeric chain

through terephthalate linkage where Cu…Cu separation is 10.83 Å (Fig. 4). These 1D chains are again interconnected through two different types C-H…π interactions (C-H…Cg, 2.98 and 3.20 Å) and finally form 2D supramolecular architecture (Figs. 5, 3S). These 2D sheets are further connected through a different type C-H…π interaction (C-H…Cg, 2.74 Å) (Table 4S) and form a 3D supramolecular network (Fig. 4S).

IR Spectra of Complexes

IR spectra of complexes are shown in Figs. 5S-7S. IR spectra show that ν(O-H) stretching vibrations appear in the region 3000-3650 cm^{-1} for all the complexes indicating the presence of lattice water molecules.[32] Stretching vibrations in the region 2975 - 2990 cm^{-1} are for C_{sp2}-H bond and bands. The spectrum of complexes exhibits band at 1641 - 1644 cm^{-1} corresponding to aliphatic ν(C=N) stretching. Aromatic ν(C=C) (for **1 - 2**) or combination of ν(C=C) and ν_{as}(OCO) (for **3**) stretching vibrations are appears in the region 1413 - 1561 cm^{-1}. The IR spectrum of complex **2** shows additional bands corresponding to $\rho_r(H_2O)$ at 741 cm^{-1} and $\rho_w(H_2O)$ at 640 cm^{-1} indicate the presence of coordinate water molecules.

Electronic absorption and emission spectra of complexes

The electronic spectra of complexes **1**, **2** and **3** were recorded in methanol. The spectrum of **1** (Fig. 8S) shows a significant transition at 215 nm ($\varepsilon \sim 8.4 \times 10^4$ liter $mole^{-1}$ cm^{-1}), 238 nm ($\varepsilon \sim 5.6 \times 10^4$ liter $mole^{-1}$ cm^{-1}), 258 nm ($\varepsilon \sim 4.6 \times 10^4$ liter $mole^{-1}$ cm^{-1}) and 343 nm ($\varepsilon \sim 1.0 \times 10^4$ liter $mole^{-1}$ cm^{-1}). For the spectrum of **2** (Fig. 8S) shows a significant transitions occur at 232 nm ($\varepsilon \sim 1.5 \times 10^5$ liter $mole^{-1}$ cm^{-1}), 270 nm ($\varepsilon \sim 1.2 \times 10^5$ liter $mole^{-1}$ cm^{-1}) and 370 nm ($\varepsilon \sim 2.2 \times 10^4$ liter $mole^{-1}$ cm^{-1}). On the other hand the electronic spectrum of complex for **3**, shows three significant transitions (Fig. 8S) are at 232 nm ($\varepsilon \sim 1.29 \times 10^5$ liter $mole^{-1}$ cm^{-1}), 273 nm ($\varepsilon \sim 5.4 \times 10^4$ liter $mole^{-1}$ cm^{-1}), and 370 nm ($\varepsilon \sim 1.0 \times 10^4$ liter $mole^{-1}$ cm^{-1}).

Result of the study of luminescence properties are summarized in Table 3. All the complexes exhibit red shifted emission. On excitation at 343 nm complex **1** exhibits luminescence bands at 425 nm (Fig. 9S) with a fluorescence quantum yield $\Phi_s = 0.39$. For **2**, λ_{ex}, 370 nm; λ_{em}, 404, 430, 451 nm and $\Phi_s = 0.51$. For **3**, λ_{ex}, 370 nm; λ_{em}, 448 nm and $\Phi_s = 0.37$. The positions of emission bands remain unchanged when λ_{ex} is varied between (λ_{ex}- 10) and (λ_{ex}+ 10) nm.

Magnetic properties of complexes

The $\chi_M T$ versus T curves for complexes **1** and **2** are shown in Fig. 6. The $\chi_M T$ versus T curve for complex **1** shows a room temperature value of 1.49 cm^3Kmol^{-1}, in agreement with the value of 1.48 cm^3Kmol^{-1} expected for four uncoupled $S = ½$ spins assuming $g = 2$, and it decreases continuously until a value of 0.18 cm^3Kmol^{-1} is reached at 10 K. Below this temperature and down to 5 K, the $\chi_M T$ value decreases smoothly, showing the tendency to form a plateau at a value between 0.18 and 0.16 cm^3Kmol^{-1}. Below 5 K, the curve drops further and faster down to a value of 0.14 cm^3Kmol^{-1} at 2 K. On the other hand, the $\chi_M T$ versus T curve for complex **2** shows a room temperature value of 1.28 cm^3Kmol^{-1}, slightly lower than the value expected for four uncoupled $S = ½$ spins assuming $g = 2$, and it decreases continuously down to 25 K, trying to form a plateau at a value close to 0 below this temperature. This behavior evidences an overall antiferromagnetic interaction in both complexes, and suggests the presence of impurities with a spin different than 0, resulting in the formation of the plateau in the $\chi_M T$ versus T curves at values different than 0~~, as well as in the sudden increase of the susceptibility χ at low temperatures in the χ versus T plot shown in Fig. 6~~.

Complex **1** presents a cubane-like structure characterized by a $[Cu_4O_4]$ core that possesses four short and two long Cu···Cu distances as a result of the particular relative arrangement of the axial axes and equatorial planes of the Cu(II) ions, leading to a [4+2] geometric type of cubane compounds proposed by Ruiz et al.[33] The corresponding equatorial or axial character of the

bridging atoms with respect to the two connected Cu(II) ions in each pair is shown in Fig. 7A. Taking this structural arrangement in consideration, the magnetic behavior of the complex can be studied by employing the isotropic spin Hamiltonian of equation 1, based on the model showed in Scheme 7B.

$$H = -J_1 (S_1S_2 + S_1S_4 + S_2S_3 + S_3S_4) - J_2 (S_1S_3 + S_2S_4) \quad \text{eq. 1}$$

J_1 describes the magnetic exchange coupling between the four Cu(II) pairs with short Cu···Cu distances, while J_2 instead characterizes the magnetic exchange coupling between the remaining two Cu(II) pairs with long Cu···Cu distances. The $\chi_M T$ versus T curve of complex **1** was fitted with the PHI program.[34] Although the four Cu(II) ions are not equivalent in the crystal, the same g value was assigned to all of them after considering their similarities. For the spin Hamiltonian described in equation 1, a good agreement with the experimental curve was found with the following parameters: g = 2.14, J_1 = -20.2 cm^{-1} and J_2 = -1.7 cm^{-1}. In addition, 15% of impurities with an S = 1 ground state had to be also considered in order to fairly reproduce the experimental data. The presence of such impurities is most likely due to the co-crystallization of ferromagnetic Cu(II) dimeric species with complex **1**. Temperature-independent paramagnetism (TIP) was considered equal to 120 × 10^{-6} cm^3mol^{-1}. The fitted curve is represented together with the experimental one in Fig. 6. The results of the fit are in agreement with orbital symmetry considerations and previously reported correlations: those Cu(II) pairs with short Cu···Cu distances are bridged by two different O atoms, from which one of them provides an exchange pathway formed exclusively by magnetic orbitals of both Cu(II) ions in the pair, leading to a significant antiferromagnetic interaction due to an efficient orbital overlap. On the contrary, Cu(II) pairs characterized by a long Cu···Cu distance always involve a non-magnetic orbital in any of their bridging pathways, and consequently the interaction is much weaker in these cases. Thus, J_1 is expected to be more negative than J_2 in [4+2] cubane systems, as observed experimentally in this work. In addition, and according to

the work of Tercero *et al.*,[35] the sign and magnitude of the J_1 magnetic exchange constant in [4+2] type of cubane compounds should correlate with the Cu-O-Cu angle characteristic of the short exchange pathway made exclusively by magnetic orbitals. In fact, calculations suggest that antiferromagnetic interactions can be expected in $[Cu_4O_4]$ compounds with angles larger than ca. 103°, in which case the overlapping of magnetic orbitals becomes effective. This correlation justifies the results obtained for complex **1**, being the value of the J_1 magnetic exchange constant equal to -20.2 cm^{-1}, in agreement with a range of θ values between 109° and 113° in the magnetic core of the complex.

Complex **2** belongs to a specific type of [4+2] cubane compounds where one of the two long Cu···Cu distances is formed by a Cu(II)-Cu(II) pair not connected through a bridging ligand, and thus their magnetic exchange can be neglected. These types of core systems are known as double-open cubane structures. Their structural arrangement and their corresponding equatorial or axial character of the bridging atoms with respect to the two connected Cu(II) ions in each pair is shown in Fig. 7C. Based on this, the magnetic behavior of the complex can be studied by employing the isotropic spin Hamiltonian of equation 2, which derives from the model, showed in Scheme 7D.

$$H = -J_1 (S_1S_3 + S_2S_4) - J_2 (S_1S_2 + S_3S_4) - J_3S_1S_4 \qquad \text{eq. 2}$$

In this case, and due to the particular double-open structure that forces a different coordination number and environment in the four Cu(II) ions, the latter can no longer be considered magnetically equivalent as in the case of complex **1**, and as a consequence the magnetic exchange coupling characteristic of the four short Cu···Cu distances is split into two clearly different constants, here described by J_1 and J_2. J_3 instead describes the magnetic exchange established through the only Cu(II)-Cu(II) bridged pair showing long distance.

The $\chi_M T$ versus T curve of complex **2** was fitted with the PHI program.[36] In this case, two g values were considered in the analysis: one for the octahedral Cu1 and Cu4 ions and one for the Cu2 and Cu3 ions with a square based pyramid geometry. In order to avoid over parametrization in the analysis, J_3 was assumed to be null, which seems reasonable considering the magnetic results and symmetry considerations described regarding the analogous J_2 of complex **1**. For the spin Hamiltonian described in equation 2, a good agreement with the experimental curve was found with the following parameters: g_1 = 2.14, g_2 = 2.12, J_1 = -54.8 cm^{-1}, J_2 = -15.9 cm^{-1} and J_3 = 0 cm^{-1} for complex **2**. In addition the fit was improved when considering the presence of a 3% Cu(II) mononuclear impurity. Temperature-independent paramagnetism (TIP) was considered equal to 120 × 10^{-6} cm^3mol^{-1}. The fitted curve is represented together with the experimental one in Fig. 6.

As in the case of complex **1**, the sign and magnitude of J_1 and J_2 magnetic exchange constants in complex **2** should correlate with the corresponding Cu-O-Cu angles formed exclusively by equatorial Cu-O bonds. The value of this angle determines the degree of overlapping between the two magnetic orbitals of the Cu(II) ions in the pair, and thus it is critical in determining the exchange constant value. In the complexes reported in this work, the largest antiferromagnetic constant J_1 describes the magnetic coupling in two Cu(II) pairs that show large Cu-O-Cu angles of 118.99° and 122.12°. The other two Cu(II) pairs show smaller Cu-O-Cu angles of 107.55° and 107.95°, and the magnetic analysis indicates an overall weaker antiferromagnetic interaction in this case, with the J_2 constant much smaller than the J_1. As expected from the magneto-structural correlation reported by Tercero *et al.*,[35] the larger the Cu-O-Cu angle, the stronger the antiferromagnetic coupling in the pair. Additionally, the antiferromagnetic nature of the two constants agrees well with the reported cross over angle of 103°, below which a ferromagnetic exchange would be operative, as observed by some of us in a previous work as well as by some other authors.[37]

The $\chi_M T$ versus T curve for complex **3** is shown in Fig. 8. It shows a room temperature value of 0.81 cm^3Kmol^{-1}, slightly higher than the value of 0.75 cm^3Kmol^{-1} expected for two uncoupled S = ½ spins assuming g = 2. This value is maintained constant down to ca. 20 K, and below this temperature the curve drops fast until a value of 0.62 cm^3Kmol^{-1} is reached at 2 K. The experimental data confirm the presence of a very weak antiferromagnetic interaction in the complex. Complex **3** consists of one dimensional polymeric chains formed by the linkage of the asymmetric dinuclear unit shown in Fig. 4. Neighbouring dinuclear units are bridged by terephthalate ions and thus long Cu···Cu inter-dinuclear distances of the order of 10 Å are observed, which predicts a negligible inter-dinuclear magnetic coupling within the chains. By assuming this hypothesis, the analysis of the magnetic data of complex **3** can be carried out by using a simple dinuclear model with the ~~an~~isotropic Hamiltonian of the type: $H = -J(S_1S_2)$, where J describes the magnetic exchange operating between the two Cu(II) ions in the asymmetric dinuclear unit. The $\chi_M T$ versus T curve of complex **3** was fitted with the PHI program.[36] A single g value was considered in the analysis and the temperature-independent paramagnetism (TIP) was considered equal to 60×10^{-6} cm^3mol^{-1}. A good agreement with the experimental curve was found with the following parameters: g = 2.08 and J = -0.5 cm^{-1}. The fitted curve is represented together with the experimental one in Fig. 8. The results of the fit confirm the very weak antiferromagnetic coupling between Cu(II) ions in the dinuclear unit, which might be expected considering that the two Cu(II) ions are bridged by two carboxylate groups with axial non-magnetic orbitals involved in both exchange pathways. This situation drastically diminishes the overlap between magnetic orbitals of the two ions making the exchange very weak or almost negligible, as experimentally observed in complex **3**.

Protein Binding Studies

Serum albumins have significant roles in drug delivery to the sites of disease, in maintenance of osmotic pressure and also function as storage protein.[38] It is therefore important to study the

interactions of biologically active metal complexes with these transport proteins as binding to these proteins may provide paths for drug transportation.[39] Interactions of metal complexes with SAs are also very important for their bio-distribution, toxicity, and even for their mechanism of action.[40] To understand the mechanism of interaction between **1**-**3** and SAs absorption titration experiments and fluorescence quenching experiments have been performed.

Absorption spectral studies

The UV-vis absorption spectroscopy of SAs in presence of complexes offers a simple way to explore the type of interaction. For a dynamic process the fluorophore and the quencher come into contact during the transient existence of the excited state, whereas static interaction refers to the formation of fluorophore-quencher complex in the ground state.[41] Fig. 10S shows the UV-visible spectra of SAs in the absence and presence of the complexes, which indicated that the absorption intensity of BSA and HSA were enhanced with a little blue shift (8 nm, 11 nm for **1**; 7 nm, 6 nm for **2**; 5 nm, 6 nm for **3** respectively) as the complexes were added (up to 13.36 μM), indicating the existence of a static interactions between SAs and the tested complexes.[41b] The apparent association constant (K_a) were calculated (Fig. 11S) using the following equation.

$$\frac{1}{(A_{obs} - A_0)} = \frac{1}{(A_c - A_0)} + \frac{1}{K_a(A_c - A_0)[complex]}$$

The plot of 1 / [complex] vs 1 / (A_{obs} - A_0) gives a straight line. From the ratio of the intercept to the slope the value of K_a was calculated. The values of apparent association constants (K_a) for BSA and HSA are 2.23×10^3, 3.03×10^3 (for **1**), 2.28×10^3, 6.62×10^3 (for **2**) and 1.21×10^3, 9.38×10^2 (for **3**) Table 4.

Fluorescence spectroscopic studies

The emission spectrum of SAs arises due to presence of tryptophan and tyrosine residues and an alternation in the emission spectra occurs primarily from the tryptophan residue due to changes in protein conformational, subunit association, substrate binding or denaturation.[42] Therefore, changes in emission spectral of SAs in presence of complexes can provide important information about the structure, dynamics and protein folding. Fluorescence titration experiments have been performed at room temperature using fixed concentration of SAs (0.475 µM BSA and 0.333 µM HSA) and varying the concentration of **1-3** (0-11.2 µM) in the range 290-500 nm (λ_{ex}= 280 nm). The change of fluorescence spectra of SAs upon gradual addition of 20µL, 0.3475 mm complexes solution are shown in Figs. 9, 12S. The fluorescence intensity of BSA at ~340 nm quenched with a small hypsochromic shift (62.17 %, 3 nm for **1**; 90.28 %, 4 nm for **2**; 65.36 %, 3 nm for **3**). The emission band of HSA at ~330 nm also quenched with blue shift (39.58 %, 6 nm for **1**; 67.70 %, 7 nm for **2**; 62.16 %, 6 nm for **3**). From the observed hypochromicity with hypsochromic shift has revealed that all the complexes bind with the SAs and the active site of the protein presence in a hydrophobic environment.[43]

From the Stern-Volmer equation[21] a linear relationship were obtained for the titration of serum albumins using complexes as a quencher (inset of Figs. 9, 12S). The calculated values of Stern-Volmer quenching constant (K_{SV}) and quenching rate constant (K_q) for BSA binding are $K_{SV} = 1.50\times10^5$, $K_q = 3.00\times10^{13}$ for **1**; $K_{SV} = 7.76\times10^5$, $K_q = 1.55\times10^{14}$ for **2** and $K_{SV} = 1.42\times10^5$, $K_q = 2.84\times10^{13}$ for **3**. Whereas for HSA binding $K_{SV} = 1.46\times10^5$, $K_q = 2.92\times10^{13}$ for **1**; $K_{SV} = 1.86\times10^5$, $K_q = 3.72\times10^{13}$ for **2** and $K_{SV} = 5.78\times10^4$, $K_q = 1.15\times10^{13}$ for **3** (Table 4). The values of Kq are 1000-fold higher than the maximum optical collision constant (2×10^{10} $M^{-1}S^{-1}$) of various kinds of quenchers to biopolymers. It suggested that quenching of SAs in presence of copper(II) complexes is occurs via a static quenching mechanism.[44]

As all the complexes bind with SAs in a static mode, the equilibrium binding constant (K_{bin}) and number of binding site (n) were also evaluated from the plot of log $[(F_o - F)/F]$ versus log

[complex] (Fig. 10) using the Scatchard equation,[29] binding constant (K_{bin}) and the number of binding sites per albumin (n) for the complexes are given in Table 4. The calculated value of n is around 1 for all the complexes, indicating the existence of just one class of binding site to complex in SAs.

Interaction with Calf-Thymus DNA

Transition metal complexes bind to double-stranded DNA through covalent or non-covalent interactions. Non-covalent interactions with DNA involve three binding modes: electrostatic interactions, intercalative binding and groove binding.[45] The interaction of complexes **1**-**3** with calf thymus DNA (CT-DNA) were investigated with Uv-vis absorption and fluorescence methods.

Absorbance spectral studies

Electronic absorption spectral studies have been performed to observe the mode of interaction of complexes with CT-DNA. Usually intercalation between the metal complexes and DNA results in hypochromism with or without red / blue shift, on the other hand non-intercalative / electrostatic interaction cause hyperchromism.[46]

The absorption spectra of the complexes in the absence and presence of CT-DNA are shown in Fig. 11 and Fig. 13S. It is seen from the spectra that, with gradual addition of CT-DNA (20 µL, 0.3059 mmol), an appreciable decrease in absorption intensity (hypochromism) of complexes with a significant red shifts occurs of 25 %, 4 nm for **1**, at 258 nm; 9 %, 1 nm for **2** at 232 nm and 16.33 % without any significant shift for **3**, at 232 nm. These results suggest that the complexes bind to CT-DNA mainly by the intercalation mode. The plots of [DNA] / (ε_a-ε_f) versus [DNA] linear relationship were obtained (inset of Fig. 11 and Fig. 13S), and the intrinsic binding constant (K_{ib}) was calculated from the ratio of the slope to the intercept. The intrinsic binding constants (K_{ib}) were calculated to be 1.40×10^5, 2.61×10^5, and 9.22×10^4 M^{-1} (Table 5)

for complexes **1**-**3**, respectively. The values suggest that all the three complexes strongly bind with CT-DNA and the binding affinity follow the order **2**>**1**>**3**.

Competitive binding between Ethidium Bromide and Compounds

To further clarify the DNA binding affinity ability and the nature of DNA-binding mode of copper complexes, ethidium bromide displacement experiments have been performed. EB is a planer, cationic dye, and emits fluorescence at about 600 nm, in the presence of CT-DNA EB fluorescence increases around 20-fold due to its strong intercalation between the adjacent DNA base pairs.[47] CT-DNA bounded EB shows emission at 602 nm on excitation at 500 nm. Addition of a metal complex which capable to bind CT-DNA via intercalation could result in a quenching of the EB bound CT-DNA emission due to the displacement of EB from CT-DNA-EB system by the complex. The emission spectra of EB bound CT-DNA in the absence and presences of complexes were given in Fig. 12.

Upon gradual addition of Cu(II) complexes (20µL, 0.3475 mmol) to aqueous solution (5 µM) of EB bound CT-DNA in HEPES buffer (pH 7.2) at room temperature results quenching in the emission of EB bounded CT-DNA takes place. The emission band exhibited hypochromism up to 51.52 % (for **1**), 62.48 % (for **2**) and 51.43 % (for **3**) of the initial fluorescence intensity. From the observed decrease in emission intensity it has been inferred that the EB molecules are displaced from the CT-DNA binding sites by complexes.[48] From the Stern-Volmer plots (inset of Fig. 12), a linear relationship (R = 0.99) were obtained. The Stern-Volmer quenching constant (K_{sv}) values have been derived from the slope of the plot F_0/F vs [complex] and are 7.94×10^4 (for **1**), 1.40×10^5 (for **2**) and 7.52×10^4 M^{-1} (for **3**). The apparent DNA binding constant (K_{app}) values were also calculated using the equation:[41a]

$$K_{EB}[EB] = K_{app}[complex]$$

Where [complex] is the complex concentration value at a 50 % reduction in the fluorescence intensity of EB, K_{EB} ($1.0 \times 10^7\ M^{-1}$) is the DNA binding constant of EB and [EB] is the concentration of EB (5 μM). The K_{app} values for **1**-**3** were found to be 3.74×10^6, 5.54×10^6 and $3.22\times10^6\ M^{-1}$ for complexes **1**-**3** respectively (Table 5). From these observed data, it is seen that complex **2** has more binding affinities than the complex **1** and **3** which is in agreement with the results obtained from the Uv-vis spectral studies.

Conclusion

In summary, we report synthesis, crystal structures, low temperature magnetic properties and study of the interactions with BSA / HSA and CT-DNA of three polynuclear copper(II) complexes. Use of Schiff base ligand H_2L^1 with Cu(II) results close cubane core structure for **1** and slight modification of Schiff base ligand (H_2L^2) gives complex **2** with double open Cu_4O_4 cubane core structure. Whereas use of H_2L^2 in combination with terephthalate spacer formed 1D polymeric copper(II) complex (**3**). Weak C-H…π interactions result 3D supramolecular architectures of **3**. Variable temperature magnetic susceptibility measurements in the range 2 - 300 K indicate antiferromagnetic exchange coupling between copper centres in all complexes, in full agreement with the behaviour expected from their structural arrangement.

The CT-DNA and protein binding of the complexes were investigated using electronic absorption and fluorescence spectroscopic techniques. Although many authors reported polynuclear copper(II) complexes including tetranuclear cubane core but few of them discussed about interactions with bio-molecules, so all the three complexes are rare example of polynuclear copper(II) compounds which are interacts with CT-DNA / serum albumins.

Acknowledgements

The authors gratefully acknowledge the financial assistance given by the CSIR, Government of India, to Dr. Subal Chandra Manna (Project No. 01 (2743)/13/EMR-II). A. F acknowledges

financial support from the Spanish Ministerio de Economía y Competitividad (MINECO) through ~~CTQ2012-32247,~~ CTQ2015-68370-P ~~and for a Ramón y Cajal Fellowship (RYC-2010-05821)~~, and from the ~~regional~~ Generalitat de Catalunya ~~authority~~ through ~~(~~2014SGR-129~~)~~.

Supplementary information

..., ….. and … contain the supplementary crystallographic data for **1-3** respectively. These data can be obtained free of charge via http://www.ccdc.cam.ac.uk/conts/retrieving.html, or from the Cambridge Crystallographic Data Centre, 12 Union Road, Cambridge CB2 1EZ, UK; fax: (+44) 1223-336-033; or e-mail: deposit@ccdc.cam.ac.uk. Tables for intermetallic distances, coordination bond angles, C-H…π interactions; figures of crystal structure, interaction with CT-DNA, SAs, IR, NMR and electronic spectra are provided as supporting information.

References

1 (a) D. Gatteschi and R. Sessoli, *Angew.Chem.*, 2003, **115**, 278-309; (b) R. E. P. Winpenny, *Adv. Inorg. Chem.*, 2001, **52**, 1-111.

2 (a) R. H. Holm, P. Kennepohl and E. I. Solomon, *Chem. Rev.*, 1996, **96**, 2239-2314.

3 a) G. R. Newkome and E. He, C. N. Moorefield, *Chem. Rev*. 1999, **99**, 1689-1746; b) S. Leininger, B. Olenyuk and P. J. Stang, *Chem.Rev*. 2000, **100**, 853-907; c) J. Y. Lu, *Coord. Chem. Rev*. 2003, **246**, 327-347; d) A. Y. Robin and K. M. Fromm, *Coord. Chem.Rev.*, 2006, **250**, 2127-2157; e) C. J. Adams, M. A. Kurawa, M. Lusi and A. G. Orpen, *CrystEngComm*, 2008, **10**, 1790-795; f) M. Chang, M. Chung, B. S. Lee and C. H. Kwak, *J. Nanosci. Nanotechnol.*, 2006, **6**, 3338-3342; g) S. G. Kang, H. Kim and S. Bang, *Inorg. Chim. Acta*, 2013, **396**, 10-13.

4 (a) R. Wegner, M. Gottschaldt, H. Görls, E. Jäger and D. Klemm, *Chem. Eur. J.*, 2001, **7**, 2143-2157; b) M. M. Dıaz-Requejo and P. J. Pérez, *Chem. Rev.*, 2008, **108**, 3379-3394; c) A. M. Kirillov, M. V. Kirillova and A. J. L. Pombeiro, *Coord. Chem. Rev.*, 2012, **256**, 2741-2759; d) S. Löw, J. Becker, C. Würtele, A. Miska, C.Kleeberg, U. Behrens, O. Walter and S. Schindler, *Chem. Eur. J.*, 2013, **19**, 5342-5351; e) E. Safaei, A. Wojtczak, E. Bill and H. Hamidi, *Polyhedron*, 2010, **29**, 2769-2775; f) E. Safaei, M. M.Kabir, A. Wojtczak, Z. Jaglicic, A. Kozakiewicz and Y. I. Lee, *Inorg.Chim.Acta*, 2011, **366**, 275-282.

5 (a) V. H. Crawford, H. W. Richardson, J. R. Wasson,D. J. Hodgson and W. E. Hatfield, *Inorg.Chem.*, 1976, **15**, 2107-2110; (b) J. Sletten, A. Sørensen, M. Julve and Y. Journaux, *Inorg. Chem.*, 1990, **29**, 5054-5058; (c) E. Ruiz, P. Alemany, S. Alvarez and J. Cano, *J. Am. Chem. Soc.*, 1997, **119**, 1297-1303; (d) J. K. Eberhardt, T. Glaser, R. -D. Hoffmann, R. Fröhlich and E. -U. Würthwein, *Eur. J. Inorg. Chem.*, 2005, 1175-1181; (e) Y. Xie, J. Ni, F. Zheng, Y. Cui, Q. Wang, S. W. Ng and W. Zhu, *Cryst. Growth Des.*, 2009, **9**, 118-126; (f) R. Papadakis, E. Rivière, M. Giorgi, H. Jamet, P. Rousselot-Pailley, M. Réglier, A. J. Simaan and T. Tron, *Inorg. Chem.*, 2013, **52**, 5824-5830.

6 (a) R. H. Holm, P. Kennepohl and E. I. Solomon, *Chem.Rev.*, 1996, **96**, 2239-2314; (b) I. A. Koval, P. Gamez, C. Belle, K. Selmeczi and J. Reedijk, *Chem. Soc. Rev.*, 2006, **35**, 814-840.

7 R. Mergehenn and W. Haase, *ActaCrystallogr., Sect. B:Struct. Crystallogr.Cryst. Chem.*, 1977, **33**, 1877-1882.

8 E. Ruiz, A. Rodríguez-Fortea, P. Alemany and S. Alvarez, *Polyhedron*, 2001, **20**, 1323-1327.

9 (a) E. I. Solomon, U. M. Sundaram and T. E. Machonkin, *Chem. Rev.*, 1996, **96**, 2563-2606; (b) E. I. Solomon, M. J. Baldwin and M. D. Lowery, *Chem. Rev.*, 1992, **92**, 521-542.

10 S. Pfaender and A. M. Grabrucker, *Metallomics*, 2014, **6**, 960-977.

11 (a) C. D. Fan, H. Su, J. Zhao, B. X. Zhao, S. L. Zhang and J. Y. Miao, *Eur. J. Med. Chem.*, 2010, **45**, 1438-1446; (b) J. D. Ranford, P. J. Sadler and D. A. Tocher, *J. Chem. Soc., Dalton*

Formatat: Espanyol (Espanya)

Trans., 1993, **22**, 3393-3399; (c) C. H. Ng, K. C. Kong, S. T. Von, P. Balraj, P. Jensen, E. Thirthagiri, H. Hamada and M. Chikira, *Dalton Trans.*, 2008, 447-454; (d) D. Yoshida, Y. Ikeda and S. Nakazawa, *J. Neuro-Oncol*., 1993, **16**, 109-115.

12 (a) T. S. Lobana, R. Sharma, G. Bawa and S. Khanna, *Coord. Chem. Rev.*, 2009, **253**, 977-1055; (b) M. Alagesan, N. S. P. Bhuvanesh and N. Dharmaraj, *Dalton Trans*., 2013, **42**, 7210-7223; (c) J. A. Lessa, I. C. Mendes, P. R. O. da Silva, M. A. Soares, R. G. dos Santos, N. L. Spezialic, N. C. Romeiro, E. J. Barreiro and H. Beraldo, *Eur. J. Med. Chem.*, 2010, **45**, 5671-5677.

13 (a) J. Costa Pessoa and I. Tomaz, *Curr. Med. Chem.*, 2010, **17**, 3701-3778; (b) T. M. Sielecki, J. F. Boylan, P. A. Benfield and G. L. Trainor, *J. Med. Chem.*, 2000, **43**, 1-18; (c) D. P. Smith, H. Chen, S. Ogo, A. I. Elduque, M. Eisenstein, M. M. Olmstead and R. H. Fish, *Organometallics*, 2014, **33**, 2389-2404.

14 (a) F. Gumus, G. Eren, L. Acik, A. Celebi, F. Ozturk, S. Yilmaz, R. I. Sagkan, S. Gur, A. Ozkul, A. Elmali and Y. Elerman, *J. Med. Chem.*, 2009, **52**, 1345-1357; (b) W. -J. Lian, X. -T. Wang, C.-Z. Xie, H. Tian, X. -Q. Song, H. -T. Pan, X. Qiao and J. -Y. Xu, *Dalton Trans.*, 2016, **45**, 9073-9087.

15 C. Santini, M. Pellei, V. Gandin, M. Porchia, F. Tisato and C. Marzano, *Chem. Rev.*, 2014, **114**, 815-862.

16 (a) A. W. Tai, E. J. Lien, M. M. Lai and T. A. Khwaja, *J. Med. Chem.*, 1984, **27**, 236-238; (b) P. H. Wang, J. G. Keck, E. J. Lien and M. M. Lai, *J. Med. Chem.*, 1990, **33**, 608-614.

17 C. Trejo-Solis, G. Palencia, S. Zuniga, A. Rodriguez-Ropon, L. Osorio-Rico, S. T. Luvia, I. Gracia-Mora, L. M. Rosado, A. Sanchez, M. E. Moreno-Garcia, A. Cruz, M. E. Bravo-Gomez, L. Ruiz-Ramirez, S. Rodriguez-Enriquez and J. Sotelo, *Neoplasia*, 2005, **7**, 563-574.

18 (a) A. Kellett, M. O'Connor, M. McCann, M. McNamara, P. Lynch, G. Rosair, V. McKee, B. Creaven, M. Walsh, S. McClean, A. Foltyn, D. O'Shea, O. Howe and M. Devereux, *Dalton*

Formatat: Espanyol (Espanya)

Trans., 2011, **40**, 1024-1027; (b) P. Shi, M. Lin, J. Zhu, Y. Zhang and Q. Jiang, *J. Biochem. Mol. Toxicol.*, 2009, **23**, 295-302; (c) R. Buchtik, Z. Travnicek and J. Vanco, *J. Inorg. Biochem.*, 2012, **116**, 163-171; (d) M. O'Connor, A. Kellett, M. McCann, G. Rosair, M. McNamara, O. Howe, B. S. Creaven, S. McClean, A. F. Kia, D. O'Shea and M. Devereux, *J. Med. Chem.*, 2012, **55**, 1957-1968.

19 (a) Y. Zhang, X. -M. Zhang, T. -F. Liu and W. -G. Xu, *Transition Met.Chem.*, 2010, **35**, 851-858; (b) Y.-F. Ji, R. Wang, S. Ding, C.-F. Du and Z.-L. Liu, *Inorg. Chem. Commun.*,2012, **16**, 47-50; (c) E. Hecht, T. Rüffer and H. Lang, *Z. Anorg.Allg.Chem.*, 2004, **630**, 1326-1329; (d) L.-X. Xie, X. Zhang, C. Yuan and X. Li, *Synth. React. Inorg., Met.-Org., Nano-Met.Chem.*, 2009, 39, 291-294; (e) X. Qin, S. Ding, X. Xu, R. Wang, Y. Song, Y. Wang, C.-f. Du and Z.-l. Liu, *Polyhedron*, 2014, **83**, 36-43; (f) A. Paul, V. Bertolasi, A. Figuerola and S. C. Manna, *J. Solid State Chem.*, 2017, **249**, 29-38.

20 D. D. Perrin, W. L. F. Armarego and D. R. Perrin, *Purification of Laboratory Chemicals*, Pergamon Press, Oxford, U.K., 1980.

21 J. R. Lakowicz, *Principles of Fluorescence Spectroscopy*, 3rd ed., Springer, NewYork, USA, 2006.

22 SMART (V 5.628), SAINT (V 6.45a), XPREP, SHELXTL, *Bruker AXS Inc*, Madison, Wisconsin, USA, 2004.

23 G. M. Sheldrick, *Siemens Area Detector Absorption Correction Program*, University of Gottingen, Gottingen, Germany, 2004.

24 A. Altomare, G. Cascarano, C. Giacovazzo and A. Guagliardi, *J. Appl. Crystallogr.*, 1993, **26**, 343-350.

25 G. M. Sheldrick, SHELXL-2014, *Program for Crystal Structure Solution and Refinement*, University of Gottingen, Gottingen, Germany, 2014.

26 L. J. Farrugia, WinGX-A Windows Program for Crystal Structure Analysis, *J. Appl. Crystallogr.*, 2012, **45**, 849-854.

27 K. Brandenburg, DIAMOND *(Version 3.2i)*, Crystal ImpactGbR, Bonn, Germany, 1999.

28 P. Smolen´ski, C. Pettinari, F. Marchetti, M. Fátima, C. Guedes da Silva, G. Lupidi, G. V. B. Patzmay, D. Petrelli, L. A. Vitali and A. J. L. Pombeiro, *Inorg. Chem.*, 2015, 54, 434-440.

29 (a) J. R. Lakowicz, Fluorescence Quenching: Theory and applications, *Principles of Fluorescence Spectroscopy*, Kluwer Academic/Plenum Publishers, New York, 1999, pp. 53-127; (b) X.-Z. Feng, Z. Lin, L.-J.Yang, C. Wang and C.-L. Bai, *Talanta*, 1998, **47**, 1223-1229.

30 A. Wolfe, G. H. Shimer and T. Mechan, *Biochemistry*, 1987, **26**, 6392-6396.

31 A. W. Addison, T. N. Rao, J. Reedijk, J. Van Rijn and G. C. Verschoor, *J. Chem.Soc., Dalton Trans.*, 1984, 1349-1356.

32 K. Nakamoto, *Infrared Spectra of Inorganic and Coordination Compounds*, John Wiley & Sons, New York, 1997.

33 E. Ruiz, A. Rodríguez-Fortea, P. Alemany and S. Alvarez, *Polyhedron*, 2001, **20**, 1323-1327.

34 N. F. Chilton, R. P. Anderson, L. D. Turner, A. Soncini and K. S. Murray, *J. Comput. Chem.*, 2013, **34**, 1164-1175.

35 J. Tercero, E. Ruiz, S. Alvarez, A. Rodríguez-Fortea and P. Alemany, *J. Mater. Chem.*, 2006, **16**, 2729-2735.

36 N. F. Chilton, R. P. Anderson, L. D. Turner, A. Soncini and K. S. Murray, *J. Comput. Chem.*, 2013, **34**, 1164-1175.

37 (a) S. C. Manna, S. Manna, A. Paul, E. Zangrando, A. Figuerola, S. Dolai and K. Das, *ChemistrySelect*, 2017, **2**, 3317-3322; (b) E. A. Buvaylo, V. N. Kokozay, O. Y. Vassilyeva, B. W. Skelton, J. Jezierska, L. C. Brunel and A. Ozarowski, *Inorg. Chem.*, 2005, **44**, 206-216.

Formatat: Espanyol (Espanya)

Formatat: Espanyol (Espanya)

Formatat: Espanyol (Espanya)

38 (a) A. R. Timerbaev, C. G. Hartinger, S. S. Aleksenko and B. K. Keppler, *Chem. Rev.*, 2006, **106**, 2224-2248; (b) W. Villarreal, L.Colina-Vegas, C. R. de Oliveira, J. C. Tenorio, J. Ellena, F. C. Gozzo, M. R. Cominetti, A. G. Ferreira, M. A. B. Ferreira, M. Navarro and A. A. Batista, *Inorg. Chem.*, 2015, **54**, 11709-11720; (c) D. C. Carter and J. X. Ho, *Adv. Protein Chem.*, 1994, **45**, 153-203.

39 (a) A. Tarushi, X. Totta, C. P. Raptopoulou, V. Psycharis, G. Psomas and D. P. Kessissoglou, *Dalton Trans.*, 2012, **41**, 7082-7091; (b) E. Ramachandran, D. S. Raja, N. S. Bhuvanesh and K. Natarajan, *Dalton Trans.*, 2012, **41**, 13308-13323.

40 J. Kljun, I. Bratsos, E. Alessio, G. Psomas, U. Repnik, M. Butinar, B. Turk and I. Turel, *Inorg. Chem.*, 2013, **52**, 9039-9052.

41 (a) E. Ramachandran, D. S. Raja, N. P. Rath, K. Natarajan, *Inorg.Chem.*, 2013, **52**, 1504-1514; (b) D. S. Raja, N. S. P. Bhuvanesh and K. Natarajan, *Inorg. Chem.*, 2011, **50**, 12852-12866.

42 Y. Wang, H. Zhang, G. Zhang, W. Tao and S. Tang, *J. Lumin.*, 2007, **126**, 211-218.

43 (a) P. Krishnamoorthy, P. Sathyadevi, A. H. Cowley, R. Butorac and N. Dharmaraj, *Eur. J. Med. Chem.*, 2011, **46**, 3376-3387; (b) P. Sathyadevi, P. Krishnamoorthy, R. Butorac, A. H. Cowley, N. S. P. Bhuvanesh and N. Dharmaraj, *Dalton Trans.*, 2011, **40**, 9690-9702; (c) P. Krishnamoorthy, P. Sathyadevi, A. H. Cowley, R. Butorac and N. Dharmaraj, *Dalton Trans.*, 2012, **41**, 6842-6854; (d) D. S. Raja, N. S. P. Bhuvanesh and K. Natarajan, *Eur. J. Med. Chem.*, 2011, **46**, 4584-4594.

44 M. R. Eftink and C. A. Ghiron, *Anal. Biochem.*, 1981, **114**, 199-227.

45 (a) F. Dimiza, S. Fountoulaki, A. N. Papadopoulos, C. A. Kontogiorgis, V. Tangoulis, C. P. Rapatopoulou, V. Psycharis, A. Terzis, D. P. Kessissoglou and G. Psomas, *Dalton Trans.*, 2011, **40**, 8555-8568; (b) S. Tsiliou, L. Kefala, F. Perdih, I. Turel, D. P. Kessissoglou and G. Psomas, *Eur. J. Med. Chem.*, 2012, **48**, 132-142; (c) A. Tarushi, X. Totta, C. P. Rapatopoulou,

Formatat: Espanyol (Espanya)

V. Psycharis, G. Psomas and D. P. Kessissoglou, *Daton Trans.*, 2012, **41**, 7082-7091; (d) A. Tarushi, X. Totta, A. Papadopoulos, J. Kijun, I. Turel, D. P. Kessissoglou and G. Psomas, *Eur. J. Med. Chem.*, 2014, **74**, 187-198; (e) M. Zampakou, N. Rizeq, V. Tangoulis, A. N. Papadopoulos, F. Perdih, I. Turel and G. Psomas, *Inorg. Chem.*, 2014, **53**, 2040-2052.

46 (a) Q.-L. Zhang, J.-G. Liu, H. Chao, G.-Q. Xue and L.-N. Ji, *J. Inorg. Biochem.*, 2001, **83**, 49-55; (b) Z.-C. Liu, B.-D. Wang, B. Li, Q. Wang, Z.-Y. Yang, T.-R. Li and Y. Li, *Eur. J. Med. Chem.*, 2010, **45**, 5353-5361; (c) F. Mancin, P. Scrimin, P. Tecilla and U. Tonellato, *Chem. Commun.*, 2005, 2540-2548; (d) L. Tjioe, A. Meininger, T. Joshi, L. Spiccia and B. Graham, *Inorg. Chem.*, 2011, **50**, 4327-4339.

47 (a) F. J. Meyer-Almes and D. Porschke, *Biochemistry*, 1993, **32**, 4246-4253; (b) G. M. Howe, K. C. Wu and W. R. Bauer, *Biochemistry*, 1976, **19**, 339-347.

48 (a) K. Jeyalakshmi, Y. Arun, N. S. P. Bhuvanesh, P. T. Perumal, A. Sreekanth and R. Karvembu, *Inorg. Chem. Front.*, 2015, **2**, 780-798; (b) P. Kumar, S. Gorai, M. Kumar, B. Mondal and D. Manna, *Dalton Trans.*, 2012, **41**, 7573-7581; c) M. A. Kostiainen, J. G. Hardy and D. K. Smith, *Angew. Chem. Int. ed.*, 2005, **44**, 2556-2559.

Table 1. Crystal data and details of structure refinement of complexes 1-3

Complex	1	2	3
Empirical formula	$C_{45}H_{54}Cu_4N_4O_9$	$C_{52}H_{57}Cu_4N_4O_{21}$	$C_{32}H_{34}Cu_2N_2O_{11}$
Formula mass, g mol^{-1}	1049.08	1328.17	749.69
Crystal system	Triclinic	Monoclinic	Monoclinic
Space group	*P-1*	*P21/n*	*Pn*
a, Å	12.023(5)	15.9727(7)	9.962(5)
b, Å	12.682(5)	19.9309(8)	17.231(5)
c, Å	15.142(5)	19.0257(8)	10.455(5)
α, deg	84.707(5)	90	90
β, deg	79.368(5)	102.925(2)	114.469(5)
γ, deg	79.585(5)	90	90
V, Å^3	2227.6(15)	5903.4(4)	1633.5(12)
Z	2	4	2
$D_{(calcd)}$, g cm^{-3}	1.564	1.494	1.524

μ(Mo-Kα), mm^{-1}	1.943	1.498	1.365
F(000)	1080	2724	772
Theta range, deg	2.1-28.3	2.1-28.4	2.4-28.4
No. of collected data	105893	239901	67078
No. of unique data	11082	14761	8152
R_{int}	0.057	0.042	0.056
Observed reflns [$I > 2\sigma(I)$]	7384	11838	7209
Goodness of fit (F^2)	1.105	1.068	1.032
Parameters refined	564	738	428
*R*1, *wR*2 ($I > 2\sigma(I)$) [a]	0.0501, 0.1638	0.0456, 0.1364	0.0320, 0.0749
Residuals, e $Å^{-3}$	-0.85, 1.02	-0.79, 0.84	-0.25, 0.36

[a] $R1(Fo) = \Sigma \| |Fo| - |Fc| | / \Sigma |Fo|$, $wR2(Fo^2) = [\Sigma w (Fo^2 - Fc^2)^2 / \Sigma w (Fo^2)^2]^{½}$

Table 2. Selected bond lengths (Å) for 1-3

1		**2**		**3**	
Cu(1)-O(2)	1.891(3)	Cu(1)-O(1)	1.989(2)	Cu(1)-O(1)	1.905(3)
Cu(1)-O(3)	1.938(3)	Cu(1)- O(2)	2.423(2)	Cu(1)- O(2)	2.008(3)
Cu(1)-O(4)	1.944(3)	Cu(1)-O(3)	1.911(2)	Cu(1)-O(3)	1.957(3)
Cu(1)-O(6)	2.561(3)	Cu(1)-O(6)	1.951(2)	Cu(1)- (O)	2.553(4)
Cu(1)-N(1)	1.934(4)	Cu(1)-O(13)	2.4929(19)	Cu(1)-N(1)	1.925(3)
Cu(2)-O(4)	1.953(3)	Cu(1)-N(2)	1.939(3)	Cu(1)-O(6_b)	2.687(3)
Cu(2)-O(5)	1.887(4)	Cu(2)-O(1)	1.9477(19)	Cu(2)-O(5)	2.572(4)
Cu(2)-O(6)	1.973(3)	Cu(2)-O(017)	1.976(2)	Cu(2)-O(6)	1.953(3)
Cu(2)-O(7)	2.504(3)	Cu(2)-O(13)	1.9353(18)	Cu(2)-O(7)	2.022(3)
Cu(2)-N(2)	1.947(4)	Cu(2)-O(14)	2.314(2)	Cu(2)-O(8)	1.901(3)
Cu(3)-O(3)	2.578(4)	Cu(2)-N(1)	1.945(3)	Cu(2)-O(3_a)	2.545(3)
Cu(3)-O(6)	1.935(3)	Cu(3)-O(6)	1.938(2)	Cu(2)-N(2_a)	1.922(4)
Cu(3)-O(7)	1.944(3)	Cu(3)-O(7)	1.982(2)		
Cu(3)-O(9)	1.896(3)	Cu(3)-O(8)	1.9416(17)		
Cu(3)-N(3)	1.933(4)	Cu(3)-O(9)	2.296(3)		
Cu(4)-O(3)	1.956(3)	Cu(3)-N(3)	1.945(3)		
Cu(4)-O(4)	2.607(3)	Cu(4)-O(6)	2.5098(19)		
Cu(4)-O(7)	1.928(3)	Cu(4)-O(8)	2.0103(19)		
Cu(4)-O(11)	1.882(4)	Cu(4)-O(10)	2.382(2)		
Cu(4)-N(4)	1.946(4)	Cu(4)-O(11)	1.902(2)		
		Cu(4)-O(13)	1.948(2)		
		Cu(4)-N(4)	1.942(2)		

Table 3. Electronic absorption and emission spectra of complexes

	Absorption / λ (nm); ε (M^{-1} cm^{-1})	Emission (nm)	Δν[a], nm	Φ_s
1	215 (8.4 × 10^4), 238 (5.6 × 10^4), 258 (4.6 × 10^4),**343** (1.0 × 10^4)	425	82	0.39
2	232 (1.5 × 10^5), 270 (1.2 × 10^5), **370** (2.2 × 10^4)	404, 430, 451	34, 60, 81	0.51
3	232(1.29× 10^5), 273 (5.4× 10^4),**370** (1.0× 10^4)	448	78	0.37

Bold number indicates the excitation wavelengths.[a]Stoke shift

Table 4. Quenching Constant (K_q), binding Constant (K_{bin}), number of binding sites (n) and apparent association constant (K_a) for the interactions of complexes with BSA and HSA

	Complexes	$K_{sv}(M^{-1})$	$k_q(M^{-1}S^{-1})$	K_{bin} (M^{-1})	n	$K_a(M^{-1})$
BSA	**1**	1.50×10^5	3.00×10^{13}	5.99×10^4	1.37	2.23×10^3
	2	7.76×10^5	1.55×10^{14}	1.48×10^5	1.61	2.28×10^4
	3	1.42×10^5	2.84×10^{13}	1.03×10^5	1.13	1.21×10^3
HSA	**1**	1.46×10^5	2.92×10^{13}	1.23×10^5	0.99	3.03×10^3
	2	1.86×10^5	3.72×10^{13}	1.48×10^5	1.15	6.62×10^3
	3	5.78×10^4	1.15×10^{13}	7.94×10^4	0.87	9.38×10^2

Table 5. Emission and absorption spectral parameters of the Cu(II) complexes bound to CT-DNA

	λ_{max} (nm)	change in emission	Δε (%)	$K_{sv}(M^{-1})$	K_{app} (M^{-1})	K_{ib} (M^{-1})
1	602	hypochromism	51.52	7.94×10^4	3.74×10^6	1.40×10^5
2	602	hypochromism	62.48	1.40×10^5	5.54×10^6	2.61×10^5
3	602	hypochromism	51.43	7.52×10^4	3.22×10^6	9.22×10^4

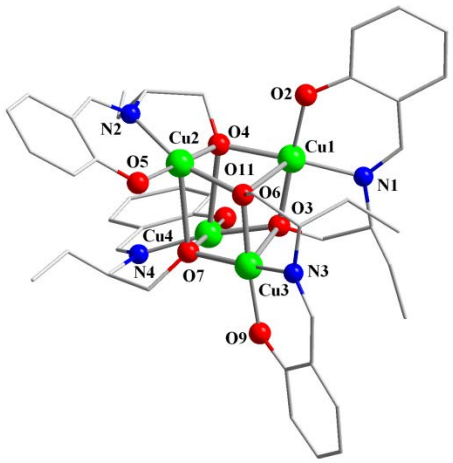

Fig. 1 Molecular structure of tetranuclear cubane in **1** with labeling of selected atoms. The lattice water molecule and hydrogen atoms have been omitted for clarity.

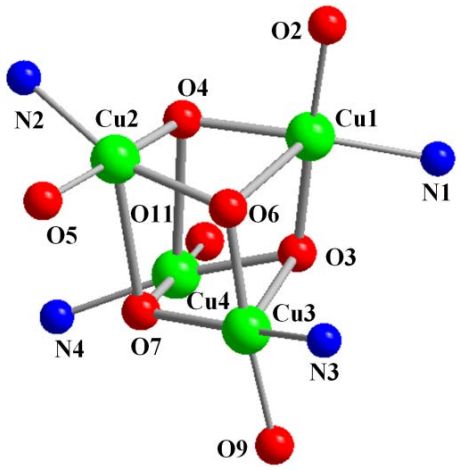

Fig. 2 Representation of the tetranuclear copper(II) core in **1** with the coordination environment of the copper(II) centers.

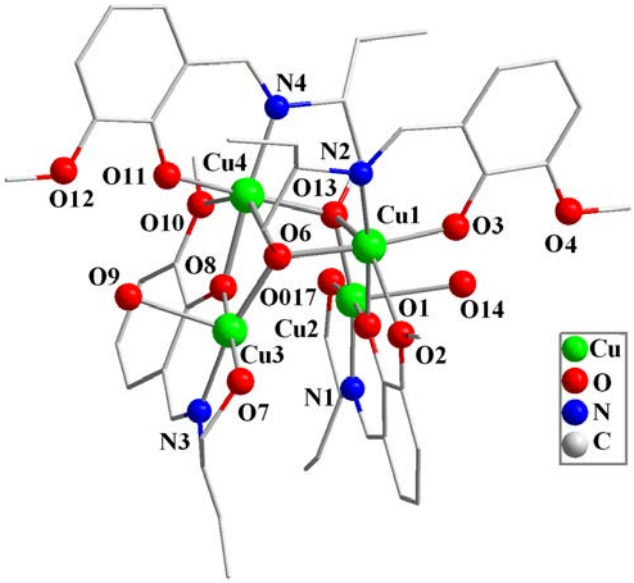

Fig. 3 Molecular structure **2** with labeling of selected atoms. The lattice water, lattice squarate molecule and hydrogen atoms have been omitted for clarity.

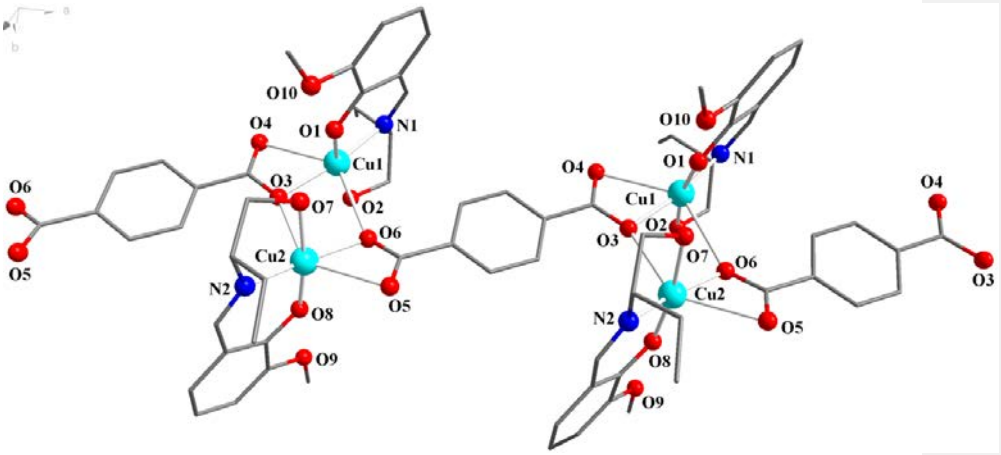

Fig. 4 The 1D polymeric structure of complex **3**. The lattice water molecule and hydrogen atoms have been omitted for clarity.

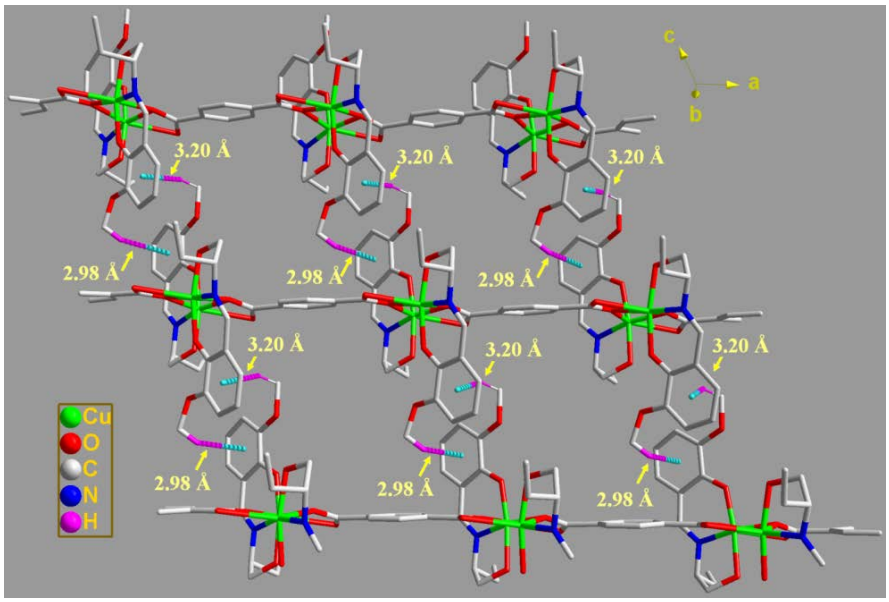

Fig. 5 2D supramolecular sheet formed by the C-H…π interaction in complex **3**.

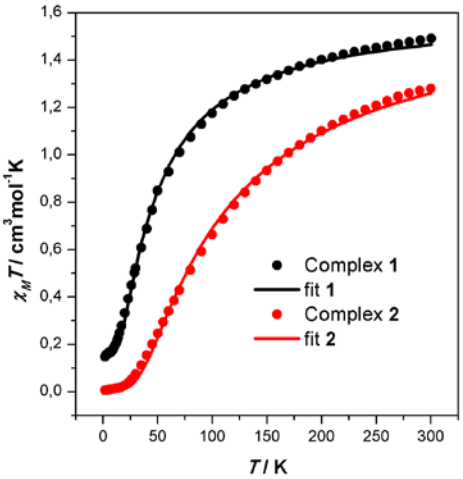

Fig. 6 Thermal dependence of the $\chi_M T$ for complexes **1** and **2**. The straight lines are the fits obtained considering the magnetic models of **Fig. 7** and using the Hamiltonian and parameters mentioned in the text.

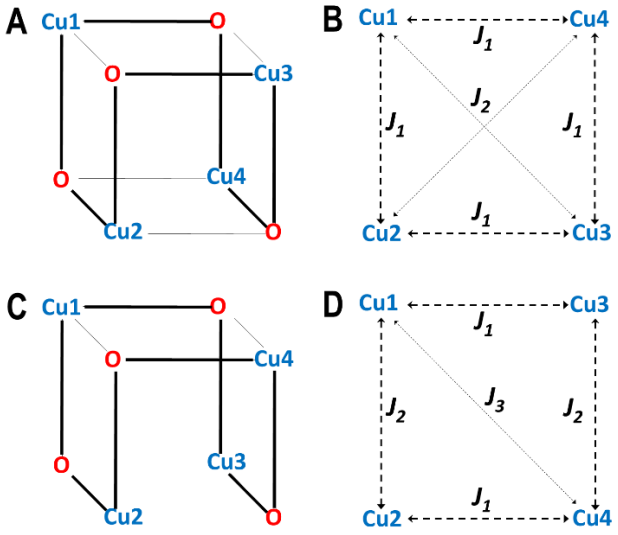

Fig. 7 A) Structural arrangement of a [4+2] cubane structure like the one of complex **1**, where short (equatorial) and long (axial) Cu-O bonds have been illustrated with thick and thin lines, respectively. B) Exchange coupling model used for the magnetic analysis of complex **1**. C)

Structural arrangement of a [4+2] double-open cubane structure like the one of complex **2**, where short (equatorial) and long (axial) Cu-O bonds have been illustrated with thick and thin lines, respectively. D) Exchange coupling model used for the magnetic analysis of complex **2**.

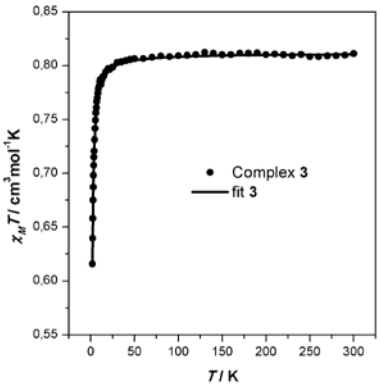

Fig. 8 Thermal dependence of the $\chi_M T$ for complex **3**. The straight line represents the fit obtained considering a Cu(II) dinuclear model and using the Hamiltonian and parameters mentioned in the text.

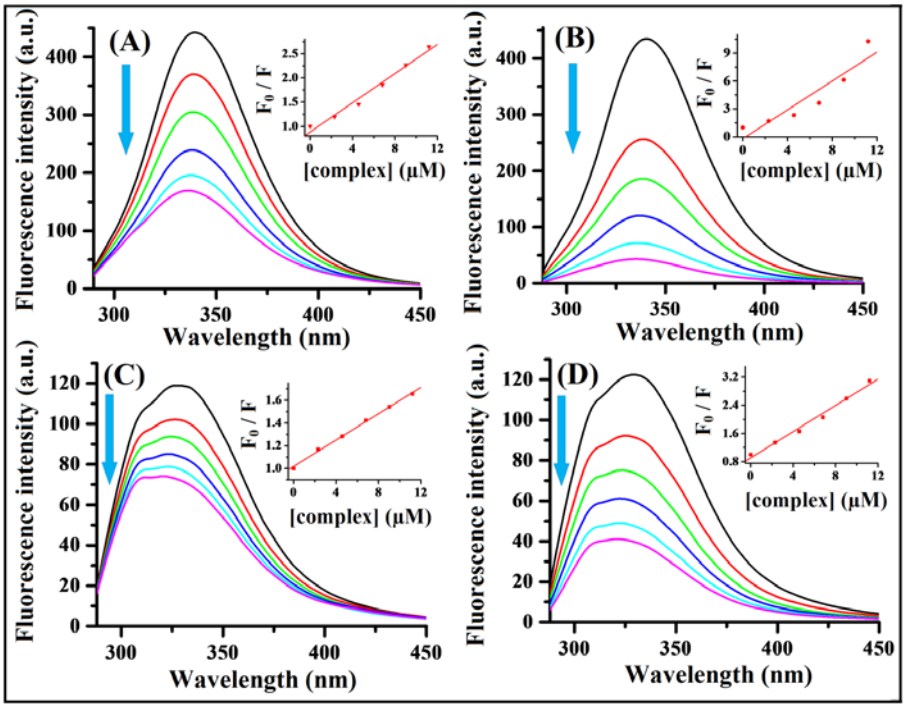

Fig. 9 Emission spectrum of BSA (λ_{ex} = 280 nm; λ_{em} = 340 nm) and HSA (λ_{ex} = 280 nm; λ_{em} = 330 nm) in the presence of increasing amounts (0 - 11.2 μM) of complexes **1** (A, C) and **2** (B, D). Arrow shows that the emission intensity changes upon increasing complex concentration. Inset: Stern-Volmer plot.

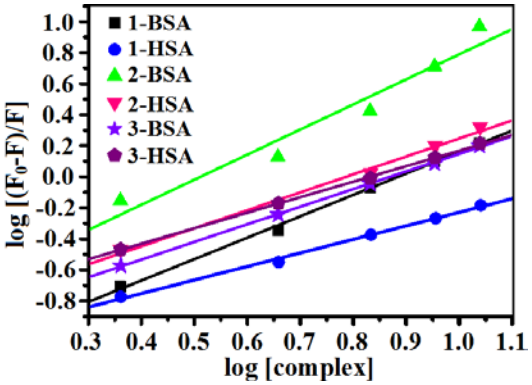

Fig. 10 Scatchard plots of the SAs fluorescence titration for complexes.

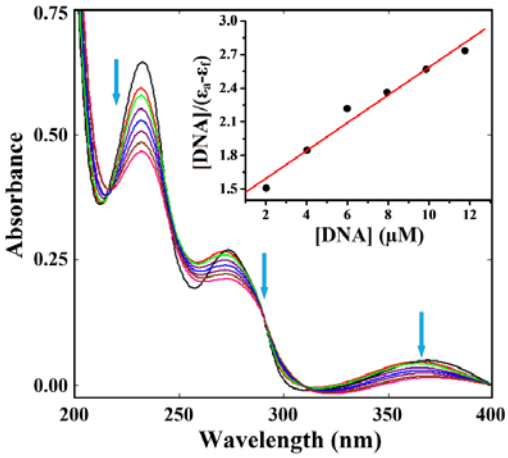

Fig. 11 Absorption titration spectra of complex **3** in the absence (black line) and presence (other lines) of CT-DNA to complex at room temperature. Inset: Plot of [DNA]/(ε_a-ε_f) versus [DNA]. Arrow shows the absorbance changes upon increasing CT-DNA concentration

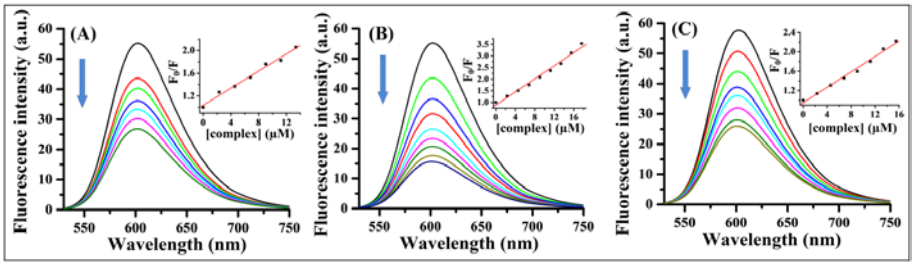

Fig. 12 Emission spectra of EB bounded CT-DNA in the presence of complex **1** (A), **2** (B) and complex **3** (C). Inset: Stern-Volmer plot of fluorescence titrations.